LETTER

Heterogeneous Electrochemical Ammonia Oxidation with a Ru-bda Oligomer Anchored on Graphitic Electrodes via CH−π Interactions

Anna M. Beiler, Alisa Denisiuk, Jan Holub, Francisco-Javier Sánchez-Baygual, Marcos Gil-Sepulcre, Mehmed Z. Ertem,* Dooshaye Moonshiram, Alberto Piccioni, and Antoni Llobet*

Read Online

ACCESS | Metrics & More | Article Recommendations | SI Supporting Information

ABSTRACT: Molecular catalysts can promote ammonia oxidation, providing mechanistic insights into the electrochemical N_2 cycle for a carbon-free fuel economy. We report the ammonia oxidation activity of carbon anodes functionalized with the oligomer $\{[Ru^{II}(bda\text{-}\kappa\text{-}N^2O^2)(4,4'\text{-}bpy)]_{10}(4,4'\text{-}bpy)\}$, **Rubda-10**, where bda is [2,2'-bipyridine]-6,6'-dicarboxylate and 4,4'-bpy is 4,4'-bipyridine. Electrocatalytic studies in propylene carbonate demonstrate that the Ru-based hybrid anode used in a 3-electrode configuration transforms NH_3 to N_2 and H_2 in a 1:3 ratio with near-unity faradaic efficiency at an applied potential of 0.1 V vs $Fc^{+/0}$, reaching turnover numbers of 7500. X-ray absorption spectroscopic analysis after bulk electrolysis confirms the molecular integrity of the catalyst. Based on computational studies together with electrochemical evidence, ammonia nucleophilic attack is proposed as the primary pathway that leads to critical N−N bond formation.
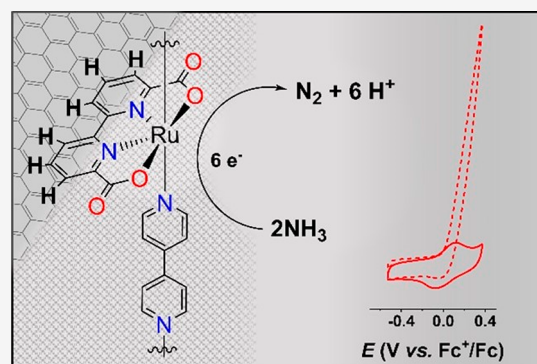
Ammonia can be liquified at room temperature under 10 bar pressure or at −33 °C in atmospheric pressure, making it an attractive hydrogen carrier with an already existing global distribution infrastructure.[1,2] Furthermore, it is a promising carbon-free renewable fuel with a high energy density for fuel cells.[3,4] For the latter, efficient and selective electrochemical ammonia oxidation (AO) to N_2 at ambient temperature and pressure is imperative. AO, like water oxidation, requires the management of multiple electrons and protons to form a bond between two heteroatoms resulting in a gaseous product. The formal potential for AO to N_2 in water is 0.092 V vs NHE at pH 0, over 1 V milder than that of water oxidation (eq 1).[5]

$$N_2 + 6e^- + 6H^+ \leftrightharpoons 2NH_3$$
$$E^\circ = +0.092 \text{ V vs. NHE (pH = 0)} \qquad (1)$$
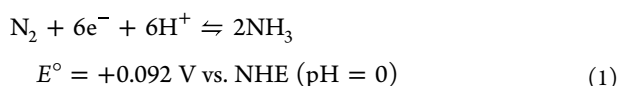
The similarities have spurred initial investigations to repurpose molecular water oxidation catalysts for AO. Molecular complexes that have shown activity as AO electrocatalysts are mainly based on Ru, Fe, and Cu metals and have been reported in the homogeneous phase. Table 1 gathers their relevant catalytic parameters.[6−14] From a technological perspective it is important to use solid-state anodes for catalytic AO, since it greatly simplifies device

engineering. Therefore, it is paramount to develop the chemistry for anchoring these molecular catalysts onto conductive surfaces, an endeavor which up to now has not been extensively pursued. Only one example in the literature reports a molecular complex for AO anchored on the surface of an ITO electrode although it displays limited activity toward AO and no product analysis is reported (Table 1, entry 4).[13] For this reason, we decided to focus our efforts on anchoring molecular complexes for AO catalysis onto conductive surfaces in order to uncover the key parameters that govern heterogeneous AO catalysis with molecular complexes.

We previously reported a Ru-bda based oligomer $\{[Ru^{II}(bda\text{-}\kappa\text{-}N^2O^2)(4,4'\text{-}bpy)]_{10}(4,4'\text{-}bpy)\}$, **Rubda-10**, where bda is [2,2'-bipyridine]-6,6'-dicarboxylate and 4,4'-bpy is 4,4'-bipyridine), that when anchored to carbon nanotubes displays a high activity for water oxidation (255 mA cm^{-2} at 1.45 V vs NHE at pH 7).[15,16] An integral part of its superior

Table 1. Key Parameters Describing Molecular Catalyst Performance for the Electrocatalytic Oxidation of Ammonia

entry	catalyst	solvent	[NH$_3$] (M)	E_{app} (V vs Fc$^{+/0}$)	TOF (s^{-1})[a]	TON	FE (%)	k_{obs}[b]	proposed mechanism[c]	ref
1	[Ru(tpy)(dmabpy)NH$_3$]$^{2+}$	THF	0.34	0.20	3.8 × 10^{-4} (10800)	4	86 (N$_2$); 78 (H$_2$)	–	ANA (hdz)	6
2	[Ru(bda)(isq)$_2$]	MeCN	0.03	–	–	–	–	0.5 s^{-1} (S)	I2N (ntd)	7
3	[Ru$_2$(μ-chp)$_4$(TfO)]	MeCN	0.64	0.00	5.6 × 10^{-2} (90)	5	52	–	ANA (hdz)	8
4	[Ru(naph-tpy)(Me$_2$N-bpy)Cl]$^+$	THF	0.34	0.08	–	–	–	–	–	13
5	[Ru(tda-κ-N^{3}O)(py$_2$)]	MeCN	2.00	0.85	2.0 × 10^{-4} (39600)	7.5	74	3.7 × 10^7 M^{-1} s^{-1} (F)	ANA (hdz)	14
6	[Fe(TPA)(NH$_3$)$_2$]$^{2+}$	MeCN	0.065	1.10	2.5 × 10^{-4} (64800)	16	80 (N$_2$) 70 (H$_2$)	1.8 × 10^9 M^{-1} s^{-1} (F)	–	9
7	[Fe(bpyPy$_2$Me)(MeCN)$_2$]$^{2+}$	MeCN	0.04	0.85	8.6 × 10^{-4} (172800)	149	87 (N$_2$)	50 M^{-1} s^{-1} (S)	–	10
8	[FeCp*(1,2-Ph$_2$PC$_6$H$_4$NH)(NH$_3$)]$^+$	THF	0.05	0.22	1.5 × 10^{-4} (28800)	4.4	74 (N$_2$) 67 (H$_2$)	0.2 M^{-1} s^{-1} (S)	ANA (hdz)	11
9	[iPr$_2$NNF$_6$]Cu^{I}–NH$_3$	MeCN	1.3	0.0	1.9×10^4 (95400)	18.2	84 (N$_2$); 74 (H$_2$)	–	I2N (hdz)	12
10	Rubda-10@CP	PC	0.012	0.10	1.9 (4055)	7500	100	4 s^{-1} (S)	ANA (ntd)	tw[d]
11	Rubda-10@CP	H$_2$O, pH 9.7	0.40	0.7 (V vs NHE)	1.6 (1226)	1990	–	16 s^{-1} (S)	–	tw[d]

[a] TOFs calculated from BEs (total time in seconds in parentheses). [b] Calculated using Shain's (S) equations or by FOWA (F). [c] ANA, ammonia nucleophilic attack; I2N, interaction of two M–N units); hdz, hydrazine pathway; ntd, nitride pathway. [d] Key: tw, this work. Ligand abbreviations used: tpy, terpyridine; dmabpy, 4,4'-bis(dimethylamino)-2,2'-bipyridine; bpy, 2,2'-bipyridine; py, pyridine; bda, [2,2'-bipyridine]-6,6'-dicarboxylate); isq, isoquinoline; chp, 6-chloro-2-hydroxypyridinate; TfO$^-$, triflate; naph-tpy, 4'(2-naphthyl)-2,2':6',2''-tpy; Me$_2$N-bpy, 4,4'-dimethylamino-2,2'-bipyridine; tda, 2,2':6',2''-terpyridine-6,6''-dicarboxylate; TPA, tris(2-pyridylmethyl)amine; bpyPy$_2$Me, 6-(1,1-di(pyridin-2-yl)ethyl)-2,2'-bipyridine; iPr$_2$NNF$_6$, diketiminato ligand.

performance compared to other molecular water oxidation catalysts immobilized on conductive surfaces is due to the high stability stemming from multiple CH−π interactions between the catalysts and the surface. Here we use a similar anchoring strategy and show that the immobilized molecular catalyst promotes heterogeneous NH$_3$ oxidation to N$_2$ with unprecedented FE (close to 100%) and TONs (7500).

We have anchored the **Rubda-10** oligomer onto carbon paper (CP) electrodes forming **Rubda-10@CP** (Figure 1).
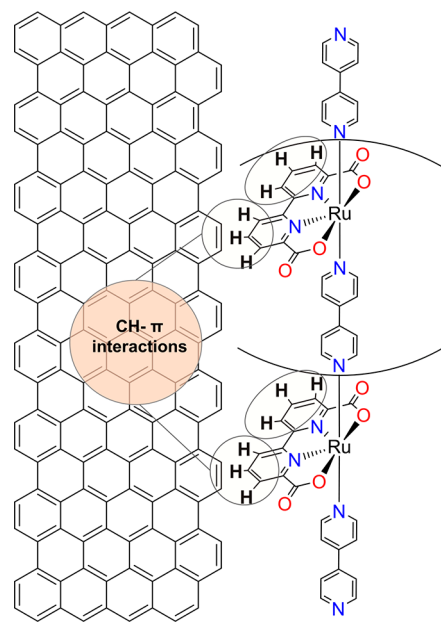

Figure 1. Drawn structure of the Rubda-10 oligomer anchored on CP to form Rubda-10@CP. The CH−π interactions are highlighted.

These molecular electrodes were characterized spectroscopically by X-ray absorption near edge spectroscopy (XANES) and extended X-ray absorption fine structure (EXAFS) spectroscopy (Figure 2, Figures S3 and S4, and Tables S1– S3). The EXAFS spectra obtained for **Rubda-10** as a powder and anchored as **Rubda-10@CP** are very similar with four long (≈2.1 Å) and two short (1.9 Å) bonding distances (Table S2) in agreement with a tetragonally distorted octahedral type of symmetry. This, together with the electrochemical experiments, indicates that the anchored oligomer maintains its structure on the graphitic surface. The XANES spectra of **Rubda-10** powder and **Rubda-10@CP** differ with half edge values of 22127.5 and 22128.5 eV that correspond to oxidation states of 2 and 2.6, respectively. The latter indicates that 60% of the original Ru(II) centers have been oxidized to Ru(III) by aerial oxygen. As described previously,[17] this is due to the exposure of Ru centers throughout the monolayer to oxygen, unlike the bulky oligomeric powder where only superficial Ru centers have access to aerial oxygen,[18] and is corroborated by an increase of 90−120 mV in the average open circuit potential of **Rubda-10@CP** electrodes left in air for 3 weeks (Table S4).

Cyclic voltammetry (CV) of **Rubda-10@CP** (Γ_{Ru} = 0.42 nmol cm^{-2}) in aqueous solution at pH 7 shows two redox events at $E_{1/2}$ = 0.69 and 0.87 V vs NHE (Figure 3a, solid line) corresponding to the formal potentials of the Ru$^{III/II}$ and Ru$^{IV/III}$ couples, respectively, similar to those found for the monomer [Ru(bda)(py)$_2$] (0.73 and 0.89 V vs NHE,
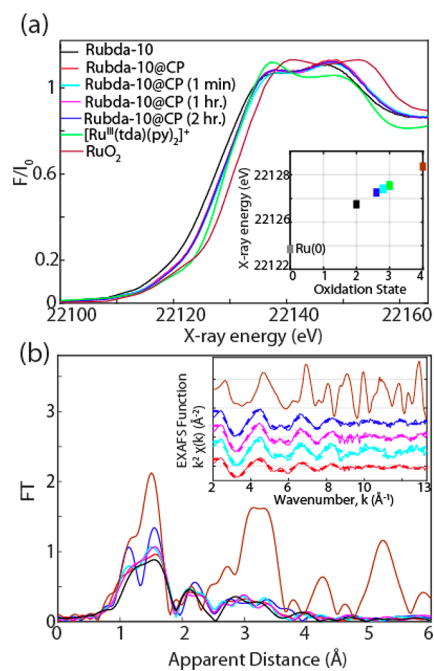
Figure 2. (a) Normalized Ru K-edge XANES for Rubda-10 complex in powder form (black),[15] Rubda-10@CP (red), after CPE for 1 min (cyan), 1 h (magenta), and 2 h (blue), together with $[Ru^{III}(tda)(py)_2]^+$ as a reference complex[17] (green) and RuO_2 (brown). The Rubda-10 complex was diluted with boron nitride pressed between a 3 μm polypropylene film and mylar tape while the hybrid complexes were pressed between two kapton tapes. All complexes were measured at 20 K in a continuous helium flow cryostat at ambient pressure and recorded in fluorescence mode using a 13-element energy resolving Ge detector (see Supporting Information for details). (Inset) Plot of half peak k-edge energy vs oxidation state. The gray square corresponds to the half edge energy of ruthenium metal powder. (b) Fourier transforms of k^2-weighted Ru EXAFS of Rubda-10 (black), Rubda-10@CP (red), after BE for 1 min (cyan), 1 h (magenta), 2 h (blue) and RuO_2 (brown). (Inset) Back-Fourier transformed experimental (solid lines) and fitted (dashed lines) $k^2[\chi(k)]$ of Ru complexes together with RuO_2. Experimental spectra were calculated for k values of 2.0−13.3 Å^{-1}.

Figure 3. (a) Cyclic voltammograms of Rubda10@CP (Γ_{Ru} = 0.42 nmol cm^{-2}) in the absence (solid) and presence (dashed) of 0.8 M NH$_3$ at a scan rate of 100 mV s^{-1} in a 0.1 M phosphate buffer solution (μ = 0.1 M). (b) Bulk electrolysis of Rubda-10@CP (red, Γ_{Ru} = 0.27 nmol cm^{-2}) and CP (black) in the presence of 0.4 M NH$_3$ at an E_{app} = 0.7 V vs NHE over 1200 s. (c) Cyclic voltammograms of Rubda-10@CP (Γ_{Ru} = 0.33 nmol cm^{-2}) in the absence (solid) and presence (dashed) of 20 mM NH$_3$ at a scan rate of 100 mV s^{-1} in PC containing 0.2 M TBAPF$_6$. (d) Bulk electrolysis of Rubda-10@CP (red, Γ_{Ru} = 0.24 nmol cm^{-2}) and CP (black) in the presence of 12 mM NH$_3$ in PC containing 0.2 M TBAPF$_6$ at an E_{app} = 0.1 V vs Fc$^{+/0}$ over 1.1 h.

respectively) in homogeneous phase under similar conditions.[15] In the presence of 0.8 M NH$_3$ the pH shifts to 10.0, and an electrocatalytic current takes off at 0.62 V vs NHE (j = 0.1 mA/cm^2) at the foot of the Ru$^{III/II}$ couple (Figure 3a, dashed line) which implies an overpotential of 1.1 V (E^o = −0.50 V vs NHE at pH = 10). The electrocatalytic rate constant for the oxidation of ammonia, k_{obs}, was calculated using Shain's equation.[19−21] A k_{obs} of 16 s^{-1} was obtained using scan rates from 40 to 150 mV s^{-1} (Figures S6 and S7). This is a lower limit value since the electrocatalytic response is not strictly in the "S-shaped" kinetic regime.[22]

The CV in propylene carbonate (PC) of **Rubda-10@CP** (Γ_{Ru} = 0.33 nmol cm^{-2}, Figure 3c, solid line) using 0.2 M TBAPF$_6$ as supporting electrolyte shows broad and overlapped waves associated with the Ru$^{III/II}$ and Ru$^{IV/III}$ couples ($E_{1/2}$ = 0.1 V vs Fc$^{+/0}$). In the presence of 20 mM ammonia, an electrocatalytic current takes off at the foot of the Ru$^{III/II}$ couple (Figure 3c, dashed line). The replacement of 0.2 M TBAPF$_6$ by 0.2 M NH$_4$PF$_6$ as supporting electrolyte gives a practically identical response (Figure S16). In propylene carbonate, the formal potential for NH$_3$ oxidation has not
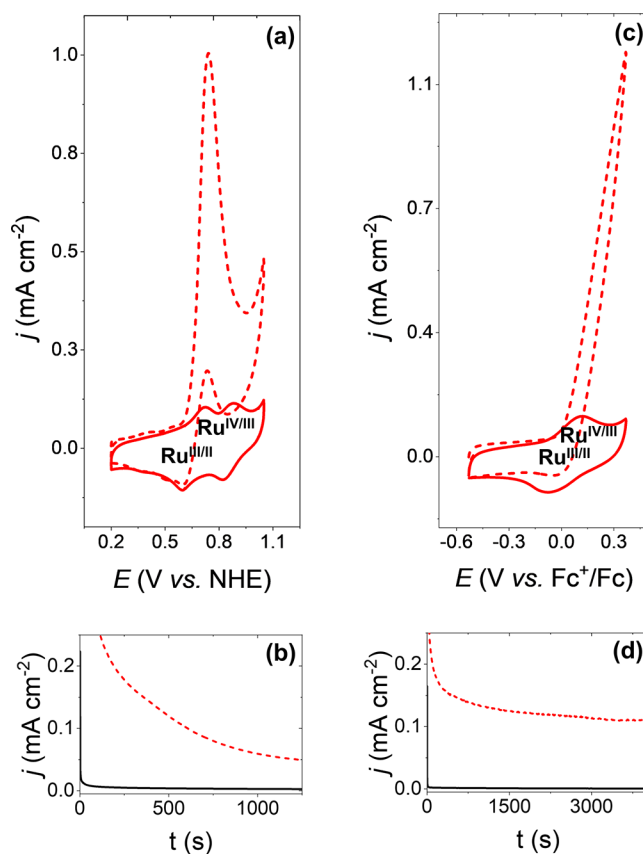
been established although it has been measured in acetonitrile[23] and tetrahydrofuran (THF).[24] Using that of THF (E^o = −0.81 V vs Fc$^{+/0}$) gives an overpotential of 0.83 V (j = 0.1 mA cm^{-2} at 0.02 V vs Fc$^{+/0}$). A k_{obs} of 4 s^{-1} was obtained using Shain's equation with scan rates of 40−200 mV s^{-1} (Figures S10 and S11). The catalytic current changes linearly with NH$_3$ concentration up to 17 mM after which additional NH$_3$ does not change the current intensity, indicating electrocatalytic saturation (Figure S12).

To spectroscopically characterize the **Rubda-10** oligomer anchored on a graphitic surface, we deposited it onto a transparent ITO electrode coated with a graphite layer of ≈10 nm thickness. The electrode was soaked for 24 h in a 0.2 mM solution of **Rubda-10** in trifluoroethanol, generating **Rubda-10@ITO-g** (Γ_{Ru} = 0.18 nmol cm^{-2}). The CVs and UV−vis analysis of this material were carried out in the presence of 1.8 mM ammonia in PC with 0.2 M TBAPF$_6$ (Figure S17). At this low concentration of NH$_3$, the Ru$^{III/II}$ and Ru$^{IV/III}$ waves shift by ≈50 mV to more positive potentials compared to the same couples in the absence of NH$_3$. Further, under this low concentration of NH$_3$, no catalytic current is observed.
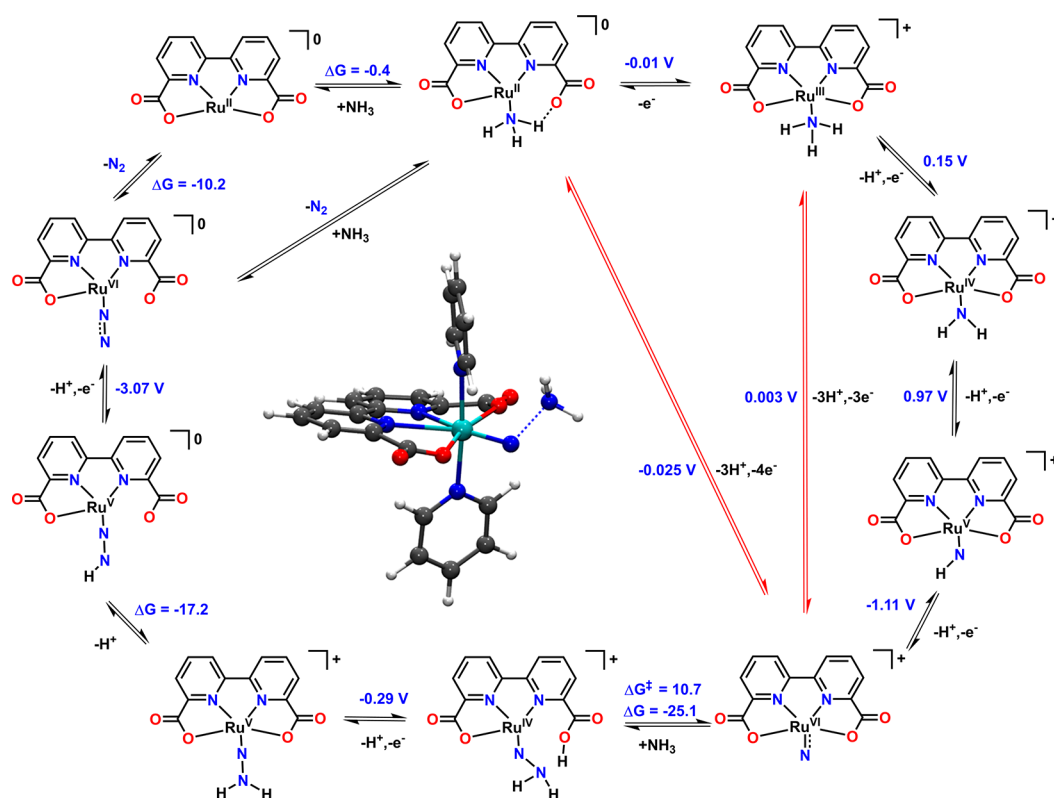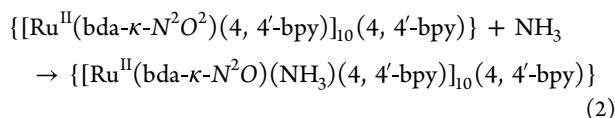
Figure 4. Computed free-energy changes (kcal mol^{-1}) and redox potentials (V vs Fc$^{+/0}$) for the proposed ammonia oxidation mechanism by $[Ru^{II}(bda\text{-}\kappa\text{-}N^2O^2)(py)_2]$. For simplicity, axial ligands are excluded in the scheme. The calculations consider the monomer unit of the oligomer replacing the bridging ligand by the terminal pyridine ligand. (Inset) Computed transition state structure for the N−N bond formation step (dashed blue line) by $[Ru^{VI}(N)(bda\text{-}\kappa\text{-}N^2O^2)(py)_2]^+$ species undergoing an ammonia nucleophilic attack (ANA). For clarity, formal oxidation states are shown for the ruthenium center.

However, when the ammonia concentration is increased 100 times to 0.18 M, a catalytic current emerges at ≈ -0.05 V vs Fc$^{+/0}$. Under the same conditions, an increase of absorbance between 350 and 550 nm is observed in the presence of NH$_3$ as compared to the same modified electrode with no ammonia present. These results together with the synthetic chemistry related to NH$_3$ substitution that occur in the $[Ru(tda\text{-}\kappa\text{-}N^3O(py_2)]$ complex,[14] suggest NH$_3$ coordination to the Ru center concomitant with decoordination of one of the bda-carboxylate groups, as indicated in eq 2 below and supported by theoretical calculations.

$$\{[Ru^{II}(bda\text{-}\kappa\text{-}N^2O^2)(4, 4'\text{-}bpy)]_{10}(4, 4'\text{-}bpy)\} + NH_3$$
$$\rightarrow \{[Ru^{II}(bda\text{-}\kappa\text{-}N^2O)(NH_3)(4, 4'\text{-}bpy)]_{10}(4, 4'\text{-}bpy)\} \quad (2)$$

Bulk electrolysis experiments were carried out in an airtight cell under argon in order to monitor catalytic longevity and product formation. In aqueous solution (0.1 M phosphate buffer) containing 0.4 M NH$_3$ (pH = 9.7), bulk electrolysis was carried out at an E_{app} = 0.7 V vs NHE for 1200 s using **Rubda-10@CP** (Γ_{Ru}= 0.27 nmol cm^{-2}) as the working electrode. A J vs. t plot (Figure 3b) shows that over time the intensity decreases from 560 to 50 μA cm^{-2}. During this period 0.31 C are passed (3.2 × 10^{-6} moles of electrons) giving a TON of 1990 assuming 100% FE. CVs of the working electrode after bulk electrolysis show little evidence of the **Rubda-10** oligomer remaining at the electrodes and points to catalyst deanchoring during catalytic operation (Figure S8). In contrast, bulk electrolysis carried out in PC shows high electrode stability.

Bulk electrolysis of **Rubda-10@CP** (Γ_{Ru}= 0.24 nmol cm^{-2}) at an E_{app} = 0.1 V vs Fc$^{+/0}$ in an airtight cell in the presence of 12 mM NH$_3$ (Figure 3d) over 1.1 h gives a charge of 1.04 C. GC analysis of the products revealed that 1.33 × 10^{-6} mol of H$_2$ and 4.85 × 10^{-7} mol of N$_2$ were produced in a 2.7:1 ratio with near-unity FE and with a calculated TON of 7500 (Figure S14).

The evolution of three working electrodes **Rubda-10@CP** (Γ_{Ru}= 0.29−0.34 mol cm^{-2}) during bulk electrolysis at E_{app} = 0.1 V vs Fc$^{+/0}$ was monitored ex-situ via cyclic voltammetry and XAS after 1 min (TON = 80), 1 h (TON = 1200), and 2 h (TON = 1760). There is little to no change in the EXAFS spectra (Figure 2, Tables S1−S3 and Figures S3 and S4) compared to the one before bulk electrolysis, indicating that the **Rubda-10** catalyst maintains its molecular integrity during catalysis. In addition, no Ru metal or RuO$_2$ was detected (Figure 2b). Cyclic voltammetry of the electrode after three hours of bulk electrolysis shows no evidence of new species being formed, further supporting the catalyst maintains its molecular identity. However, a decrease in the intensity of the catalytic wave is observed that suggests partial deanchoring of the oligomer over time (Figure S15).

Density functional theory (DFT) calculations were carried out at the MN15 level of theory[25] in order to gain further insight at a molecular level of the AO catalytic cycle associated with the anchored **Rubda-10** complex and complement the experimental data (Figure 4 and Figure S18). For computational efficiency we adopted the monomer $[Ru^{II}(bda\text{-}\kappa\text{-}N^2O^2)(py)_2]$, labeled **Rubda**, to model the NH$_3$ oxidation catalytic cycle.

The proposed mechanism starts with the binding of NH_3 to **Rubda** forming $[Ru^{II}(bda-\kappa-N^2O)(NH_3)(py)_2]$, which is slightly favored on thermodynamic grounds ($\Delta G = -0.4$ kcal mol^{-1}). This substantiates the experimental results described in eq 2, where one of the carboxylates of the bda ligand decoordinates from the metal center stabilizing a hydrogen bonding interaction with the bound ammonia ligand. Next, a single electron transfer (-0.01 V vs Fc$^{+/0}$) generates $[Ru^{III}(bda-\kappa-N^2O^2)(NH_3)(py)_2]^+$. This species has a coordination number of 6.5, with 6 Ru−N/O bonding distances and one Ru−O contact (2.48 Å) in agreement with the 18-electron rule. The CN6 homologue is only 3.8 kcal mol^{-1} higher in energy and features H-bonds between the bound Ru-NH$_3$ and the decoordinated carboxylate ($d_{H-O} = 2.01$ Å). From this point, three consecutive proton-coupled electron transfer (PCET) steps give access to the reactive Ru^{VI}−N intermediate via the formation of the corresponding amide (Ru^{IV}−NH$_2$) and imide (Ru^V−NH) species before the rate limiting N−N bond formation occurs. These intermediates are not detected experimentally since only a large electrocatalytic wave is observed at the foot of the Ru$^{III/II}$ redox couple (Figure 3c). This is consistent with the thermodynamics obtained by theoretical calculations for 3 or 4 coupled one-step processes as indicated with red arrows in the computed catalytic cycle shown in Figure 4. The following step, N−N bond formation to generate the hydrazido species $[Ru^V(Hbda-\kappa-N^2O^1)$ (N-NH$_2$)(py)$_2]^+$ via ammonia nucleophilic attack (ANA), is thermodynamically downhill by 25.1 kcal mol^{-1} and constitutes the rate-determining chemical step with an activation energy of 10.7 kcal mol^{-1}. The transition state for this step is pictured in the center of the catalytic cycle where the N−N bond formation is highlighted with dashed blue line. The pathway for N−N bond formation involving the dimerization of two Ru^V−N entities (I2N) was not considered given the limited rotational and translational mobility of the **Rubda-10** oligomer on the surface of the electrode. Additionally, the molecular rigidity of the oligomer and the long distance among consecutive Ru centers (11.4 Å) precludes intramolecular N−N bond formation. After the N−N bond formation via ANA, a series of highly favorable PCET and/or deprotonation steps lead to N$_2$ evolution, completing the catalytic cycle.

Up to now, the molecular transition metal complexes used to oxidize ammonia to nitrogen employ nonenvironmentally friendly organic solvents such as MeCN and THF and their key parameters are displayed in Table 1. Initial work in the field was carried out with $[Ru(tpy)(dmabpy)(L)]^{2+}$ (where dmabpy is 4,4′-bis(dimethylamino)-2,2′-bipyridine and L = H$_2$O or NH$_3$), $[Ru(bda)(isq)_2]$ and $[Ru(tda)(py)_2]$ complexes that are well-known water oxidation catalysts, although their performance as AO catalysts are rather poor, giving TONs in the range of 4−7 (Table 1, entries 1, 2, and 5).[6,7,14] However, this initial work has generated a rich chemistry related to Ru−NH$_3$ containing complexes including the characterization of potential reaction intermediates involved in the catalytic cycle. The field has been appreciably enriched with the recent contributions reporting two Fe complexes based on the N4 polypyridyl type of ligands $[Fe(TPA)(NH_3)_2]^{2+}$ [9] and $[(bpyPy_2Me)Fe(MeCN)_2]$[9,10] (Table 1, entries 6−7) reaching TONs of ≈150, with relatively high E_{app}, in the range of 0.85 to 1.10 V vs Fc$^{+/0}$, which implies an overpotential of ≈1.6 to 1.9 V for AO ($E^o = -0.81$ V vs Fc$^{+/0}$). Cu complexes with β-diketiminato[12] and 2-[(2,2′-bipyridin)-6-yl]propan-2-ol li-

gands[26] have also been reported to be active for AO. The former has been shown to oxidize NH$_3$ to N$_2$ in acetonitrile at an $E_{app} = 0.0$ V vs Fc$^{+/0}$ with a TON of 18.2 over 26.5 h (Table 1, entry 9).[12]

From the materials perspective, state-of-the-art electrocatalysts for AO are based on Pt metal at pH 14, typically operating at overpotentials in the range of 0.4 and 0.6 V.[27] In contrast, Ru metal has little to no activity for N$_2$ evolution from NH$_3$ oxidation, due to the formation of inactive N$_{ads}$ species on the surface.[28] However, a mix of RuO$_2$ and TiO$_2$ on a Ti electrode has been shown to promote AO in phosphate buffer with 12 mM NH$_3$ at pH 12.2, with an overpotentials of approximately 1.66 V.[29]

In conclusion, we report the first example of molecular complex anchored on a conductive surface with proven electrocatalytic activity for AO to N$_2$. The oligomeric Ru complex **Rubda-10,** anchored on carbon paper via CH−π interactions, **Rubda-10@CP**, presents an unprecedented robustness under relatively mild conditions with an $E_{app} = 0.1$ V vs Fc$^{+/0}$ displaying a sustained current density of 140 μA/cm^2 for over 1 h for AO. This implies 7500 TONs, ≈50 times higher than the best molecular catalyst reported to date. Importantly the FE is close to 100% generating N$_2$ and H$_2$ with a ratio close to 1:3 using PC as an environmentally friendly solvent. From a mechanistic perspective, we show the immobilized Ru complex initially coordinates NH$_3$ followed by a series of PCET steps before N−N bond formation occurs as evidenced by cyclic voltammetry and supported by theoretical calculations. This constitutes the first unambiguous example of an ANA mechanism given the restricted rotational and translation mobility of the Ru centers in this hybrid material. Finally, we show that the hybrid material, **Rubda-10@CP**, can also work in aqueous conditions at pH 10 giving 1990 TONs at an E_{app} of 0.7 V vs NHE over 1200 s, although its stability is poor.

Outstanding challenges still remain for molecular hybrid materials as AO catalysts, including the need to significantly increased their robustness during catalytic turnover using environmentally friendly solvents such as PC[30] and water and the need to operate the AO catalysis at a substantially lower overpotentials.

■ ASSOCIATED CONTENT

Ⓢ Supporting Information

The Supporting Information is available free of charge at https://pubs.acs.org/doi/10.1021/acsenergylett.2c02483.

> Experimental Section along with additional spectroscopic, electrochemical, and computational data (PDF)

■ AUTHOR INFORMATION

Corresponding Authors

Antoni Llobet − *Institute of Chemical Research of Catalonia (ICIQ), Barcelona Institute of Science and Technology (BIST), 43007 Tarragona, Spain; Departament de Química, Universitat Autònoma de Barcelona, 08193 Barcelona, Spain;* Ⓞ orcid.org/0000-0002-6176-5272; Email: allobet@iciq.cat

Mehmed Z. Ertem − *Chemistry Division, Energy & Photon Sciences Directorate, Brookhaven National Laboratory, Upton, New York 11973-5000, United States;* Ⓞ orcid.org/0000-0003-1994-9024; Email: mzertem@bnl.gov

Authors

Anna M. Beiler − *Institute of Chemical Research of Catalonia (ICIQ), Barcelona Institute of Science and Technology (BIST), 43007 Tarragona, Spain;* ⊙ orcid.org/0000-0003-1027-3304

Alisa Denisiuk − *Institute of Chemical Research of Catalonia (ICIQ), Barcelona Institute of Science and Technology (BIST), 43007 Tarragona, Spain*

Jan Holub − *Institute of Chemical Research of Catalonia (ICIQ), Barcelona Institute of Science and Technology (BIST), 43007 Tarragona, Spain*

Francisco-Javier Sánchez-Baygual − *Institute of Chemical Research of Catalonia (ICIQ), Barcelona Institute of Science and Technology (BIST), 43007 Tarragona, Spain*

Marcos Gil-Sepulcre − *Institute of Chemical Research of Catalonia (ICIQ), Barcelona Institute of Science and Technology (BIST), 43007 Tarragona, Spain*

Dooshaye Moonshiram − *Instituto de Ciencia de Materiales de Madrid, Consejo Superior de Investigaciones Científicas, 28049 Madrid, Spain;* ⊙ orcid.org/0000-0002-9075-3035

Alberto Piccioni − *Department of Physics and Astronomy, University of Bologna, 40127 Bologna, BO, Italy;* ⊙ orcid.org/0000-0002-3447-2650

Complete contact information is available at:
https://pubs.acs.org/10.1021/acsenergylett.2c02483

Notes

The authors declare no competing financial interest.

■ REFERENCES

(1) MacFarlane, D. R.; Cherepanov, P. V.; Choi, J.; Suryanto, B. H. R.; Hodgetts, R. Y.; Bakker, J. M.; Ferrero Vallana, F. M.; Simonov, A. N. A Roadmap to the Ammonia Economy. *Joule* **2020**, *4* (6), 1186−1205.

(2) U.S. Department of Energy*Potential Roles of Ammonia in a Hydrogen Economy*; 2006; pp 123

(3) Simons, E. L.; Cairns, E. J.; Surd, D. J. The Performance of Direct Ammonia Fuel Cells. *J. Electrochem. Soc.* **1969**, *116* (5), 556.

(4) Jiao, F.; Xu, B. Electrochemical Ammonia Synthesis and Ammonia Fuel Cells. *Adv. Mater.* **2019**, *31*, 1805173.

(5) Dunn, P. L.; Cook, B. J.; Johnson, S. I.; Appel, A. M.; Bullock, R. M. Oxidation of Ammonia with Molecular Complexes. *J. Am. Chem. Soc.* **2020**, *142* (42), 17845−17858.

(6) Habibzadeh, F.; Miller, S. L.; Hamann, T. W.; Smith, M. R. Homogeneous Electrocatalytic Oxidation of Ammonia to N 2 under Mild Conditions. *Proc. Natl. Acad. Sci. U. S. A.* **2019**, *116* (8), 2849−2853.

(7) Nakajima, K.; Toda, H.; Sakata, K.; Nishibayashi, Y. Ruthenium-Catalysed Oxidative Conversion of Ammonia into Dinitrogen. *Nat. Chem.* **2019**, *11* (8), 702−709.

(8) Trenerry, M. J.; Wallen, C. M.; Brown, T. R.; Park, S. V.; Berry, J. F. Spontaneous N2 Formation by a Diruthenium Complex Enables Electrocatalytic and Aerobic Oxidation of Ammonia. *Nat. Chem.* **2021**, *13* (12), 1221−1227.

(9) Zott, M. D.; Garrido-Barros, P.; Peters, J. C. Electrocatalytic Ammonia Oxidation Mediated by a Polypyridyl Iron Catalyst. *ACS Catal.* **2019**, *9* (11), 10101−10108.

(10) Zott, M. D.; Peters, J. C. Enhanced Ammonia Oxidation Catalysis by a Low-Spin Iron Complex Featuring Cis Coordination Sites. *J. Am. Chem. Soc.* **2021**, *143* (20), 7612−7616.

(11) Li, Y.; Chen, J.-Y.; Miao, Q.; Yu, X.; Feng, L.; Liao, R.-Z.; Ye, S.; Tung, C.-H.; Wang, W. A Parent Iron Amido Complex in Catalysis of Ammonia Oxidation. *J. Am. Chem. Soc.* **2022**, *144*, 4365.

(12) Ahmed, M. E.; Raghibi Boroujeni, M.; Ghosh, P.; Greene, C.; Kundu, S.; Bertke, J. A.; Warren, T. H. Electrocatalytic Ammonia Oxidation by a Low Coordinate Copper Complex. *J. Am. Chem. Soc.* **2022**, DOI: 10.1021/jacs.2c07977.

(13) Sévery, L.; Szczerbiński, J.; Taskin, M.; Tuncay, I.; Brandalise Nunes, F.; Cignarella, C.; Tocci, G.; Blacque, O.; Osterwalder, J.; Zenobi, R.; Iannuzzi, M.; Tilley, S. D. Immobilization of Molecular Catalysts on Electrode Surfaces Using Host−guest Interactions. *Nat. Chem.* **2021**, *13* (6), 523−529.

(14) Holub, J.; Vereshchuk, N.; Sánchez-Baygual, F. J.; Gil-Sepulcre, M.; Benet-Buchholz, J.; Llobet, A. Synthesis, Structure, and Ammonia Oxidation Catalytic Activity of Ru-NH3 Complexes Containing Multidentate Polypyridyl Ligands. *Inorg. Chem.* **2021**, *60*, 13929.

(15) Gil-Sepulcre, M.; Lindner, J. O.; Schindler, D.; Velasco, L.; Moonshiram, D.; Rüdiger, O.; Debeer, S.; Stepanenko, V.; Solano, E.; Würthner, F.; Llobet, A. Surface-Promoted Evolution of Ru-Bda Coordination Oligomers Boosts the Efficiency of Water Oxidation Molecular Anodes. *J. Am. Chem. Soc.* **2021**, *143* (30), 11651−11661.

(16) Hoque, M. A.; Gil-Sepulcre, M.; de Aguirre, A.; Elemans, J. A. A. W.; Moonshiram, D.; Matheu, R.; Shi, Y.; Benet-Buchholz, J.; Sala, X.; Malfois, M.; Solano, E.; Lim, J.; Garzón-Manjón, A.; Scheu, C.; Lanza, M.; Maseras, F.; Gimbert-Suriñach, C.; Llobet, A. Water Oxidation Electrocatalysis Using Ruthenium Coordination Oligomers Adsorbed on Multiwalled Carbon Nanotubes. *Nat. Chem. 2020 1211* **2020**, *12* (11), 1060−1066.

(17) Creus, J.; Matheu, R.; Peñafiel, I.; Moonshiram, D.; Blondeau, P.; Benet-Buchholz, J.; García-Antón, J.; Sala, X.; Godard, C.; Llobet, A. A Million Turnover Molecular Anode for Catalytic Water Oxidation. *Angew. Chemie Int. Ed.* **2016**, *55* (49), 15382−15386.

(18) Matheu, R.; Ghaderian, A.; Francàs, L.; Chernev, P.; Ertem, M. Z.; Benet-Buchholz, J.; Batista, V. S.; Haumann, M.; Gimbert-Suriñach, C.; Sala, X.; Llobet, A. Behavior of Ru−bda Water-Oxidation Catalysts in Low Oxidation States. *Chem. Eur. J.* **2018**, *24* (49), 12838−12847.

(19) Lee, K. J.; Elgrishi, N.; Kandemir, B.; Dempsey, J. L. Electrochemical and Spectroscopic Methods for Evaluating Molecular Electrocatalysts. *Nat. Rev. Chem.* **2017**, *1*, 0039.

(20) Costentin, C.; Passard, G.; Savéant, J.-M. Benchmarking of Homogeneous Electrocatalysts: Overpotential, Turnover Frequency, Limiting Turnover Number. *J. Am. Chem. Soc.* **2015**, *137* (16), 5461−5467.

(21) Nicholson, R. S.; Shain, I. Theory of Stationary Electrode Polarography. Single Scan and Cyclic Methods Applied to Reversible, Irreversible, and Kinetic Systems. *Anal. Chem.* **1964**, *36* (4), 706−723.

(22) Rountree, E. S.; McCarthy, B. D.; Eisenhart, T. T.; Dempsey, J. L. Evaluation of Homogeneous Electrocatalysts by Cyclic Voltammetry. *Inorg. Chem.* **2014**, *53* (19), 9983−10002.

(23) Lindley, B. M.; Appel, A. M.; Krogh-Jespersen, K.; Mayer, J. M.; Miller, A. J. M. Evaluating the Thermodynamics of Electrocatalytic N2 Reduction in Acetonitrile. *ACS Energy Lett.* **2016**, *1* (4), 698−704.

(24) Wang, F.; Gerken, J. B.; Bates, D. M.; Kim, Y. J.; Stahl, S. S. Electrochemical Strategy for Hydrazine Synthesis: Development and Overpotential Analysis of Methods for Oxidative N−N Coupling of an Ammonia Surrogate. *J. Am. Chem. Soc.* **2020**, *142* (28), 12349−12356.

(25) Yu, H. S.; He, X.; Li, S. L.; Truhlar, D. G. MN15: A Kohn−Sham Global-Hybrid Exchange−correlation Density Functional with Broad Accuracy for Multi-Reference and Single-Reference Systems and Noncovalent Interactions. *Chem. Sci.* **2016**, *7* (8), 5032−5051.

(26) Liu, H.; Lant, H. M. C.; Troiano, J. L.; Hu, G.; Mercado, B. Q.; Crabtree, R. H.; Brudvig, G. W. Electrocatalytic, Homogeneous Ammonia Oxidation in Water to Nitrate and Nitrite with a Copper Complex. *J. Am. Chem. Soc.* **2022**, *144* (19), 8449−8453.

(27) Rosca, V.; Duca, M.; de Groot, M. T.; Koper, M. T. M. Nitrogen Cycle Electrocatalysis. *Chem. Rev.* **2009**, *109* (6), 2209−2244.

(28) De Vooys, A. C. A.; Koper, M. T. M.; Van Santen, R. A.; Van Veen, J. A. R. The Role of Adsorbates in the Electrochemical Oxidation of Ammonia on Noble and Transition Metal Electrodes. *J. Electroanal. Chem.* **2001**, *506* (2), 127−137.

(29) Donten, M.; Hyk, W.; Ciszkowska, M.; Stojek, Z. Electro-oxidation of Ammonia and Simple Amines at Titanium Electrodes Modified with a Mixture of Ruthenium and Titanium Dioxides. *Electroanalysis* **1997**, *9* (10), 751−754.

(30) Parker, H. L.; Sherwood, J.; Hunt, A. J.; Clark, J. H. Cyclic Carbonates as Green Alternative Solvents for the Heck Reaction. *ACS Sustain. Chem. Eng.* **2014**, *2* (7), 1739−1742.

▢ Recommended by ACS

Identification of Active Sites for Ammonia Electrosynthesis on Ruthenium

Lin Hu, Xiaofeng Feng, *et al.*
NOVEMBER 04, 2022
ACS ENERGY LETTERS   READ ☑

Demonstrating the Electron–Proton-Transfer Mechanism of Aqueous Phase 4-Nitrophenol Hydrogenation Using Unbiased Electrochemical Cells

Hua An, Ning Yan, *et al.*
NOVEMBER 28, 2022
ACS CATALYSIS   READ ☑

Swinging Hydrogen Evolution to Nitrate Reduction Activity in Molybdenum Carbide by Ruthenium Doping

Ouwen Peng, Kian Ping Loh, *et al.*
NOVEMBER 28, 2022
ACS CATALYSIS   READ ☑

Role of Electronic Structure on Nitrate Reduction to Ammonium: A Periodic Journey

O. Quinn Carvalho, Kelsey A. Stoerzinger, *et al.*
AUGUST 04, 2022
JOURNAL OF THE AMERICAN CHEMICAL SOCIETY   READ ☑

Get More Suggestions >